Theor Chem Acc (2007) 117:521–533
DOI 10.1007/s00214-006-0177-2

REGULAR ARTICLE

Tailoring model Hamiltonians for dihalogen—rare gas matrix problems

A diatomics-in-molecules study of Br_2 in solid Ar

A. Borowski · O. Kühn

Received: 11 August 2006 / Accepted: 26 September 2006 / Published online: 8 November 2006

Abstract A strategy for reducing the number of electronic states which need to be incorporated into a diatomics-in-molecules description of prototypical condensed phase processes is demonstrated. The selection of a problem-adapted representation is based on symmetry properties of the molecular basis set and its disturbance by the external potential due to the environment. Using the $B \leftarrow X$ excitation of Br_2 in solid Argon as an example, we show that the energy range accessible via a Franck–Condon transition can approximately be described by 17 instead of all 36 valence states. The approach shall be particularly useful for reducing the numerical effort of semiclassical and quantum dynamics simulations.

Keywords Diatomics-in-molecules · Halogen · Rare gas matrix · Model Hamiltonian · Predissociation

1 Introduction

Based upon a simple composition and the properties of its constituent parts, dihalogen molecules embedded in rare gas matrices at low temperatures continue to draw attention as prototype condensed phase systems. From the experimental point of view it is the chromophore, spatially fixed in an inert environment, together with a broad knowledge of its gas phase spectroscopy, that allows spectroscopic investigation [1] and even coherent control [2,3] of fundamental condensed phase phenomena via optical laser pulses. From the theoretical point it is their system-bath nature that makes these systems accessible for a detailed description [5,6]. However, this is not as trivial as it seems since the dynamics often involves many electronic states which can be mixed due to the coupling to specific nuclear degrees of freedom. Consequently, a key issue is the treatment of the *relevant* interactions at a maximum of accuracy and a minimum of computational costs.

For both purposes the semiempirical diatomics-in-molecules (DIM) method has turned out to be a rather successful approach. Introduced by Ellison in 1963 [7] this method was originally designed to calculate the electronic structure of polyatomic molecules just from diatomic and atomic potentials without explicit determination of interaction integrals. Later Tully refined this method and used DIM potential energy surfaces (PES) for studying molecular collision dynamics [8,9]. Starting from the 1990s different variants of the DIM method and closely related approaches have been used especially for the simulation of the photodissociation dynamics of various halogen – rare gas (X–Rg) species. Gersonde and Gabriel [10] have studied the photodissociation of HCl and Cl_2 in Xe crystals, Lawrence and Apkarian [11] the spin–orbit transitions of I in crystalline Xe and Kr, Batista and Coker [12–14] simulated the photodissociation and recombination dynamics of I_2 in liquid and solid Xe and Ar and the defragmentation dynamics of $I_2^- Ar_n$ clusters. At about the same time Gerber et al. [15,16] investigated the nonadiabatic dissociation dynamics of HCl and F_2 in solid Ar and Grigorenko et al. [17–19] analyzed the PES as well as stability of He–Cl_2 and Ar–Cl_2 van der Waals clusters and performed simulations for Cl_2 in Ne matrices. Similarly Buchachenko et al. [20–23] worked on the triatomic X–Rg species Ne–I_2, Ar–I_2, Kr–I_2, He–Cl_2, Ar–Cl_2, and

A. Borowski · O. Kühn (✉)
Institut für Chemie und Biochemie, Freie Universität Berlin, Takustr. 3, 14195 Berlin, Germany
e-mail: ok@chemie.fu-berlin.de

He–Br_2. Some recent applications of DIM are strong field alignment studies for ClF in solid Ar and Kr [24,25], coherent phonon excitation for Cl_2 in Ar [4], and wave packet dynamics simulations on reduced dimensionality PES for ClF [26] as well as for F_2 [27,28] and Cl_2 [29] in Ar. The DIM method has also been extended to flexible molecules like I_3 [30] in Ar clusters and generalized to calculate PES for quasistationary and bound states of polyatomic anions [31].

In this contribution we investigate the system Br_2 in solid Ar, a choice which is motivated by the recent time-resolved experiments of Schwentner and coworkers on this system (see, e.g., [2,32,33]), for which no corresponding theoretical studies exist. Among the phenomena of interest are the vibrational wave packet dynamics in the electronic B state and its control by tailored laser pulses, the related effect of nonadiabatic transitions to other electronic states (predissociation), and the role of the coupling to the lattice vibrations leading, for instance, to the observation of long lasting coherent phonon vibrations.

The theoretical description of coherent vibrational wave packets moving on several electronic PES calls for a quantum treatment, which can be separated into two parts, that is, the electronic structure problem and the solution of the time-dependent Schrödinger equation. This paper solely focusses on the first aspect which is addressed using the DIM method. Although the basic idea of the DIM method, that is, a representation of a polyatomic PES by a sum of pairwise interactions, is simple, it is a semiempirical approach whose complexity depends on the number of electronic states included. Already the approximate representation of a dihalogen molecule by two interacting p-atoms gives rise to 36 covalent molecular configurations, all of them have to be incorporated when using the standard DIM approach. However, often one is interested in the PES and dynamics of particular states only. For instance, the spectroscopic experiments mentioned above address a subset of states only by virtue of the selectivity provided by the laser spectrum, e.g., the states accessible by a $B \leftarrow X$ excitation. Thus, in order to reduce the numerical overhead especially of the related dynamics simulations, it would be advantageous to have a means to account for the physically relevant states within the DIM approach only, without deteriorating the overall accuracy.

In the following we explore the possibility of reducing the dimensionality of the DIM Hamiltonian to yield a problem-adapted model Hamiltonian. In particular, a compact model containing the necessary information for the treatment of the $B \leftarrow X$ excitation in Br_2 in Argon is discussed. The paper is organized as follows. In Sect. 2 the general formalism of the DIM method is reviewed putting emphasis on halogen molecules in rare gas matrices. It is followed by details on the construction of DIM Hamiltonians in an appropriate basis set representation. Our reduction strategy is detailed in Sect. 3. It consists of three steps: first, symmetry considerations are utilized to classify and estimate different coupling types. Second, a Franck–Condon based target energy interval is defined in order to decide which electronic states to incorporate into a reduced model. Third, the effect of state reduction is carefully checked to estimate the quality and the range of applicability of the model. Section 4 summarizes our results.

2 DIM method for X_2–Rg systems

The basic idea of the DIM method is the description of a polyatomic molecule in terms of all possible pairwise interactions between its atoms [7]. It is closely connected to the valence bond (VB) concept of electron pairs forming bonds between atoms. Underlying is the heuristic idea of a spatial assignment of electrons to bonds in the molecule and consequently to single atoms for large internuclear separations. The electronic wave function of such a polyatomic "gas" could be expressed as a properly antisymmetrized product of atomic basis functions. However, already at moderate internuclear separations reactive atoms tend to interact and to share their electrons, which now may be assigned to diatomic groups. For a single X_2 guest molecule in a crystal of closed shell rare gas atoms with $^1S_0$ character the electronic wave function could be written as an antisymmetrized product of diatomic functions, representing the halogen molecule, times s-functions representing individual Rg atoms. In other words, the product ansatz for the electronic wave function facilitates the decomposition of the Hamiltonian in its matrix representation into diatomic and atomic fragments. Within the DIM method these matrix elements are parameterized by pair potentials and atomic energies.

2.1 The molecular X_2 Hamiltonian

The choice of an appropriate basis for the diatomic functions depends on the halogen species under consideration. Common to all halogen atoms is the ^2P term for the ground state with an electron hole in the p^5-shell behaving like a single electron with quantum numbers $L = 1$ and $S = \frac{1}{2}$. Russel–Saunders coupling (L, S) splits up the ^2P term into $^2P_{3/2}$ and $^2P_{1/2}$. The atomic doublet separation of the heavy halogens Br and I (3,685 and $7,603\,\mathrm{cm}^{-1}$ [34]) is larger than the dissociation energies of Br_2 and I_2 in the molecular excited states. Thus, a

spatial quantization of the J's rather than that of the individual L's appears in the electric field generated by the two nuclei (J_a, J_b-coupling). The total electronic angular momentum along the internuclear axis of the molecule, Ω, is obtained by adding the single atomic quantum numbers M_J: $\Omega = |M_{J_a} + M_{J_b}|$. This is then the only "good" quantum number, the other possible molecular quantum numbers $\Lambda = |M_{L_a} + M_{L_b}|$ and $\Sigma = |M_{S_a} + M_{S_b}|$ cannot be assigned separately (Hund's coupling case c). To every combination of two M_J values there corresponds a different molecular state, except that states differing only in the sign of both M_J's form a degenerate pair as long as $\Omega \neq 0$ [35]. A zero order approximation to the molecular wave function of a homonuclear dihalogen $X_a - X_b$ can be written as a linear combination of simple products of non-overlapping spin–orbit-coupled atomic states, $|J, M\rangle_a$ and $|J, M\rangle_b$, to account for its symmetry:

$$\psi_{\Omega}^{(X_2)} = \sum_{i}^{n_i} c_{i,\Omega} |J, M\rangle_a |J', M'\rangle_b, \tag{1}$$

where n_i is the number of different products $|J, M\rangle_a$ $|J', M'\rangle_b$ in $\psi_{\Omega}^{(X_2)}$ for a given molecular state Ω with expansion coefficients $c_{i,\Omega}$. These approximate molecular basis functions are listed in Table 1 in the Appendix, where they are ordered according to their dissociation products and classified with respect to their symmetry labels Ω_w^{σ} according to Hund's case c together with their Hund's case a ${}^{2\Sigma+1}\Lambda_w^{\sigma}$ precursors. Here σ denotes the sign of the wave function with respect to reflection on a plane containing the molecular axis and w its parity with respect to the origin. Notice that Buchachenko and Stepanov [20] have discussed alternative expressions for some Hund's case c states of the same symmetry within the same dissociation limit. A general scheme for building up these functions was given by Chang [36] and Umanskij and Nikitin [37].

Expressed in the basis of molecular electronic symmetry eigenfunctions any intramolecular interaction couples functions of the same Hund's case c symmetry only [38]. The matrix representation of the Hamiltonian would be block diagonal with respect to these symmetries, that is, it separates in the given basis into two 4×4 matrices $(0_g^+, 0_u^-)$ and two 1×1 matrices $(0_g^-, 0_u^+)$, each of them being non-degenerate as well as into two 2×2 matrices $(2_g, 2_u)$, one 3×3 matrix (1_g), one 5×5 matrix (1_u), and one 1×1 matrix (3_u), each of them being doubly degenerate (cf. Table 1). This circumstance allows us to parameterize the diagonal elements of the block matrices with the potential energy curves obtained from ab initio calculations. Such a parameterization is strictly valid only if the wave functions from ab initio calculations significantly overlap with the functions of the DIM basis [39,40]. A heuristic argument for this overlap criterion would be that the covalent excited states of a halogen molecule originate from all possible configurations derived from its $\sigma_g^2 \pi_u^4 \pi_g^4 \sigma_u^0$ molecular orbital ground state configuration and halogen valence shell p-orbitals are expected to predominantly contribute to the latter.

2.2 Construction of the X–Rg interaction Hamiltonian

In the following we consider N atoms labeled by the index $i = 1, \ldots, N-2$ for the Rg and $\alpha = a, b$ for the dihalogen. At the heart of the DIM method is the representation of the X–Rg interaction in the basis of the X_2 molecular states being defined by the molecules' electronic angular momentum and thus spatially associated with its internuclear axis. A halogen-rare gas van der Waals complex may be imagined as a p-radical interacting with a closed shell s^2p^6-atom and its resulting electronic angular momenta can be classified in terms of Σ- and Π-type interactions. In matrix representation the interaction Hamiltonian, $\mathbf{V}_R^{X_\alpha - Rg_i}$, is diagonal with respect to the p_Π-, $p_{\bar{\Pi}}$- and p_Σ-orbitals of the respective reference frame R (see Fig. 1):

$$\mathbf{V}_R^{X_\alpha - Rg_i} = \begin{pmatrix} V_\Pi & 0 & 0 \\ 0 & V_{\bar{\Pi}} & 0 \\ 0 & 0 & V_\Sigma \end{pmatrix} \tag{2}$$

The diagonal elements of this matrix can be parameterized by empirical potentials obtained from experiments that provide information on the anisotropy of the

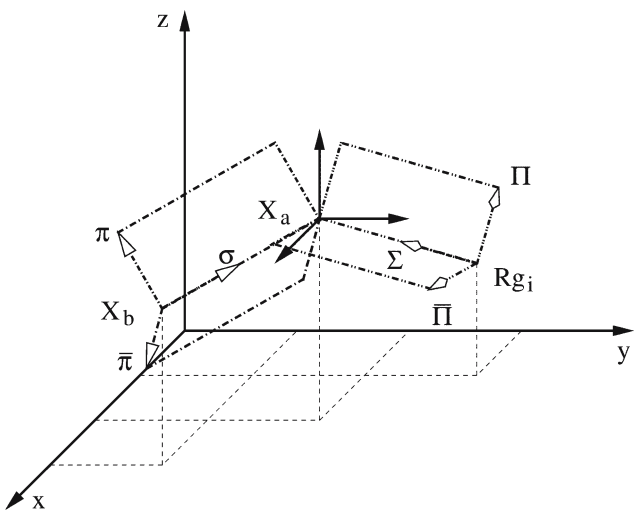

Fig. 1 Body frame transformation from the initial internal $(\Pi, \bar{\Pi}, \Sigma)$ reference frame of the X_a–Rg_i van der Waals complex (R) via a laboratory (x, y, z) frame (L) to the final internal $(\pi, \bar{\pi}, \sigma)$ reference frame (D) of the diatomic X_a–X_b molecule

interaction, such as crossed molecular beam scattering [41] or zero-electron kinetic energy photoelectron spectra [42,43]. In order to express $\mathbf{V}_R^{X_\alpha-Rg_i}$ with respect to the quantization axis of the dihalogen molecule we follow the approach of Batista and Coker (cf. Fig. 1); for details see [12]. In a first step an orthogonal matrix $\mathbf{T}_{R,L}$ transforms $\mathbf{V}_R^{X_\alpha-Rg_i}$ from its initial $(\Pi, \bar{\Pi}, \Sigma)$ frame R to the laboratory frame L representing $\mathbf{V}_L^{X_\alpha-Rg_i}$ in a basis of real p-orbitals with unique orientation:

$$\mathbf{V}_L^{X_\alpha-Rg_i} = \mathbf{T}_{R,L}\mathbf{V}_R^{X_\alpha-Rg_i}\mathbf{T}_{R,L}^{\mathrm{T}}. \tag{3}$$

Since the laboratory frame is the same for all X_α–Rg_i pairs, the $\mathbf{V}_L^{X_\alpha-Rg_i}$ can be summed up for both X-atoms separately. It is important to notice that summing up the fragment Hamiltonians in the laboratory frame can considerably save computational time as compared with a summation at the end of all further transformation steps. It appears as if this fact has been overlooked in previous work [10,12,16]. Now a second transformation is used in order to represent the corresponding partial sums on X_a and X_b in the $(\pi, \bar{\pi}, \sigma)$ body frame (D) of the dihalogen molecule. This is accomplished by another orthogonal matrix $\mathbf{T}_{L,D}$, which specifies the mutual orientation of both halogen atoms with respect to the laboratory frame and results in a new interaction operator $\mathbf{V}_D^{X_\alpha-Rg}$:

$$\mathbf{V}_D^{X_\alpha-Rg} = \mathbf{T}_{L,D}\left(\sum_{i=1}^{N-2}\mathbf{V}_L^{X_\alpha-Rg_i}\right)\mathbf{T}_{L,D}^{\mathrm{T}}. \tag{4}$$

In Fig. 1 this sequence of transformations is illustrated. Note that the second step is necessary only if a rotation of the X_2 molecule with respect to the laboratory frame needs to be taken into account explicitly, e.g., to describe librational motion.

Being expressed in the basis of real p-orbitals with the desired orientation, two more transformations are necessary to represent the halogen – rare gas interaction Hamiltonian in the basis of the spin–orbit coupled functions. First, a matrix $\mathbf{T}_{D,m_l}$ which transforms between real and complex basis functions, is applied as a unitary transformation to $\mathbf{V}_D^{X_\alpha-Rg}$ resulting in the complex representation $\mathbf{V}_{m_l}^{X_\alpha-Rg}$. In a second step the electronic spin is introduced by an outer product of $\mathbf{V}_{m_l}^{X_\alpha-Rg}$ with a 2×2 identity matrix $\mathbf{I}_2$. The resulting interaction Hamiltonian $\mathbf{V}_{m_lm_s}^{X_\alpha-Rg}$ is now defined in the basis $\{|m_l, m_s\rangle\}$:

$$\mathbf{V}_{m_lm_s}^{X_\alpha-Rg} = \mathbf{V}_{m_l}^{X_\alpha-Rg}\otimes\mathbf{I}_2. \tag{5}$$

The final step is the coupling of the electron's angular momentum and its spin by a Clebsh–Gordon matrix $\mathbf{T}_{m_lm_s,JM}$, transforming between the uncoupled $|m_l, m_s\rangle$ and the coupled representation $|J, M\rangle$, in which $\mathbf{V}_{m_lm_s}^{X_\alpha-Rg}$ can be expressed according to:

$$\mathbf{V}_{JM}^{X_\alpha-Rg} = \mathbf{T}_{m_lm_s,JM}\,\mathbf{V}_{m_lm_s}^{X_\alpha-Rg}\,\mathbf{T}_{m_lm_s,JM}^{\mathrm{T}}. \tag{6}$$

In passing we note that an alternative to this approach has been given by Buchachenko et al. [20,21], where, starting from the spin-coupled representation of the X–Rg interaction Hamiltonian and using a Jacobian coordinate system, a single Wigner rotation is applied to transform it to the X_2 quantization axis.

2.3 Representation of the atomic fragment Hamiltonians in the molecular basis

In order to express the fragment interaction Hamiltonians $\mathbf{V}_{JM}^{X_\alpha-Rg}$ of the individual halogen atoms with their joint quantization axis in a basis of molecular eigenfunctions, a tensor product with an 6×6 identity matrix $\mathbf{I}_6$ needs to be applied to both matrices:

$$\mathbf{V}_{JM_aJM_b}^{X_a-Rg} = \mathbf{V}_{JM}^{X_a-Rg}\otimes\mathbf{I}_6 \tag{7}$$

$$\mathbf{V}_{JM_aJM_b}^{X_b-Rg} = \mathbf{I}_6\otimes\mathbf{V}_{JM}^{X_b-Rg}. \tag{8}$$

This way, the Hilbert space of the molecule is introduced via the tensor product of the Hilbert spaces of both atoms. Correspondingly, its eigenfunctions can be expressed by products of atomic eigenfunctions $|J, M\rangle_a|J, M\rangle_b$. The transformation of $\mathbf{V}_{JM_aJM_b}^{X_a-Rg}$ and $\mathbf{V}_{JM_aJM_b}^{X_b-Rg}$ to a joint representation in a basis of Hund's case c VB-functions $|VB\rangle = \psi_\Omega^{(X_2)}$ is accomplished by the orthogonal transformation:

$$\mathbf{V}_{VB}^{X_2-Rg} = \mathbf{T}_{JM,VB}\left(\mathbf{V}_{JM_aJM_b}^{X_a-Rg} + \mathbf{V}_{JM_aJM_b}^{X_b-Rg}\right)\mathbf{T}_{JM,VB}^{\mathrm{T}}, \tag{9}$$

where the transformation matrix $\mathbf{T}_{JM,VB}$ contains the coefficients given in Table 1. This step allows us to consider all X_2–Rg interactions as a perturbation to the energies of the isolated halogen molecule and the assignment of matrix elements to the symmetry eigenfunctions of the unperturbed system. Thus, the total electronic Hamiltonian can be expressed as a sum of the diagonal matrix $\mathbf{H}_{VB}^{X_2}$ of the dihalogen molecule and a non-diagonal matrix $\mathbf{V}_{VB}^{X_2-Rg}$ for its interaction with the rare gas crystal. As the interaction between the Rg-atoms is independent of the electronic state of the dihalogen molecule, it contributes with the same value to each diagonal element of the total electronic Hamiltonian, to which it simply can be added after multiplication with a 36×36 identity matrix $\mathbf{I}_{36}$:

$$\mathbf{H}_{VB}^{el} = \mathbf{H}_{VB}^{X_2} + \mathbf{V}_{VB}^{X_2-Rg} + \left(\sum_{i=1}^{N-3}\sum_{j=i+1}^{N-2}V^{Rg_i-Rg_j}\right)\times\mathbf{I}_{36}. \tag{10}$$

This electronic Hamiltonian parametrically depends on all nuclear coordinates. Below we will be particularly interested in the dependence of $\mathbf{H}_{VB}^{el}$ on the coordinates of the dihalogen molecule for fixed Ar positions. Upon choosing the Hund's case *c* VB basis, $\mathbf{H}_{VB}^{X_2}$ is diagonal and includes the spin–orbit coupling. The states can be classified according to their dissociation limits (cf. Table 1). With respect to the interaction with the Rg matrix these states can be termed diabatic, whereas if the full Hamiltonian, Eq. (10), is diagonalized one obtains adiabatic states expressed as a superposition of the diabatic ones.

3 Application to Br_2 in an Ar matrix

In the following we want to apply the formalism from Sect. 2 to PES calculations for Br_2 in solid Ar. Starting from a full DIM Hamiltonian we will derive a reduced model designed such as to describe the $B \leftarrow X$ transition and subsequent (predissociation) processes. First, the matrix elements of the X_2-Hamiltonian from Sect. 2.1 are parameterized by Br_2 potential energy curves from spin–orbit coupled contracted configuration–interaction (SOCI) calculations of Yabushita [44] shown in Fig. 2.

For the representation the Br–Ar interaction we have used the results of photoelectron spectroscopic data [43] which give the spin-coupled $V_{3/2,1/2}$, $V_{3/2,3/2}$ and $V_{1/2,1/2}$ potentials. In order to set up a X–Rg-Hamiltonian according to Sect. 2.2, the spin-uncoupled V_Σ- and V_Π-potentials can be obtained according to the following the relations [45]:

$$V_\Sigma = \frac{(\frac{2}{3}\Delta + V_{3/2,1/2})V_{3/2,3/2} - (\Delta + V_{3/2,1/2})V_{3/2,1/2}}{V_{3/2,3/2} - V_{3/2,1/2} - \frac{1}{3}\Delta} \tag{11}$$

$$V_\Pi = V_{3/2,1/2}, \tag{12}$$

with Δ being the bromine spin–orbit splitting constant.

The geometry of a single Br_2 guest molecule fixed in an Ar crystal is shown in Fig. 3. It occupies a double substitutional site pointing in ⟨110⟩ direction of the face-centered cubic (fcc) Ar lattice.

For a rectangular cut-out of the crystal along this direction the molecule is surrounded by an arrangement of Ar atoms such that there is an overall D_{2h} symmetry. Starting from this situation and fixing the Ar atoms at their regular lattice positions we will consider two scenarios which we expect to be predominant at low temperatures: First, a D_{2h} symmetric elongation of the Br_2 molecule with respect to its center of mass. Second, an elongation for a configuration where the Br_2 molecular axis is tilted with respect to the ⟨110⟩ direction such that the symmetry is reduced to C_i. This situation shall illustrate the general effect of symmetry lowering, mimicking for instance, the effect of the Br_2 zero-point librational motion on the electronic couplings.

3.1 Classification of coupling types

The key step towards a reasonable reduction scheme is an investigation of the structure of the DIM Hamiltonian matrix which will lead us to its partitioning into

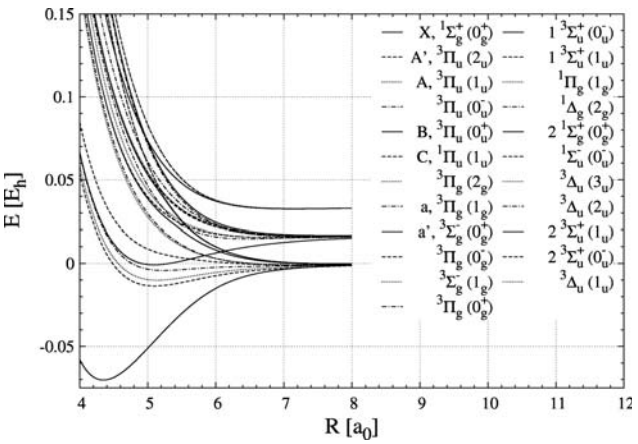

Fig. 2 Ab initio SOCI potential energy curves for the lower 23 Hund's case *c* excited states of Br_2 arising from its ground state $\sigma_g^2\pi_u^4\pi_g^4\sigma_u^0$ MO configuration [44] (see also Ref. [34]). Potential energy curves are ordered according to their Franck–Condon excitation energy from ground state minimum, Hund's case *a* and *c* labels are given in Table 1

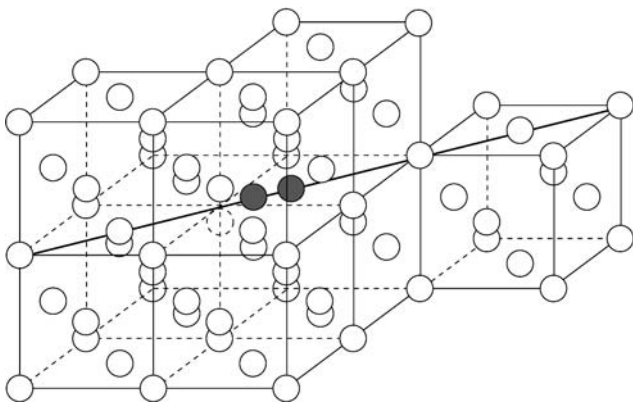

Fig. 3 Br_2 molecule (*filled circles*) in a double substitutional site pointing in ⟨110⟩ direction (*thick solid line*) of an Ar fcc lattice (*empty circles*). Periodic boundary conditions have been used for an orthorhombic box with 116 atoms. Note, that a convergence check has been performed using 968 atoms

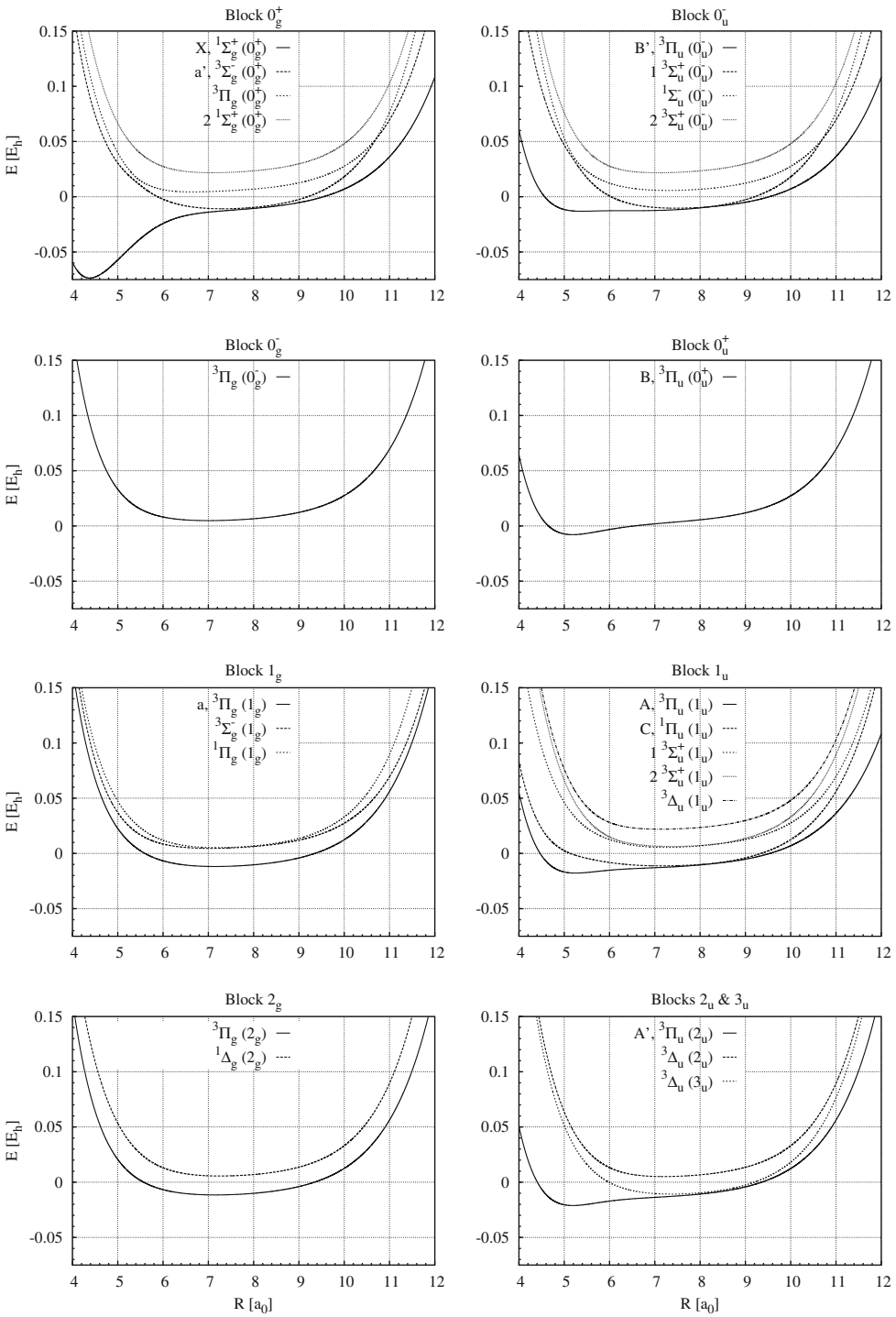

Fig. 4 Potential energy curves for the DIM valence states along the Br_2 bond distance for fixed Ar positions and D_{2h} symmetry. The data have been obtained by block-diagonalization of the Hamiltonian, thus incorporating Ω_w^σ intra-symmetric couplings in a first diagonalization step. For labeling of the states, compare Table 1

certain submatrices. Starting point is the block diagonal structure of the isolated halogen molecule's Hamiltonian in the basis of Hund's case *c* symmetry eigenfunctions (see Eq. (1) and Table 1). According to Sect. 2.3 the effect of the rare gas atoms can then be understood as a perturbation, which induces couplings among different molecular states. Regardless of its specific structure, this perturbation may be separated into components having the same symmetry or a different symmetry as compared to the isolated molecule. Such grouping can be accomplished, if we impose the isolated molecule's symmetry blocks as a mask on the total Hamiltonian matrix. Accordingly, the off-diagonal elements within a single block of given symmetry may be called *intra-symmetric* couplings. They couple the corresponding diagonal elements (molecular potential energy curves) among

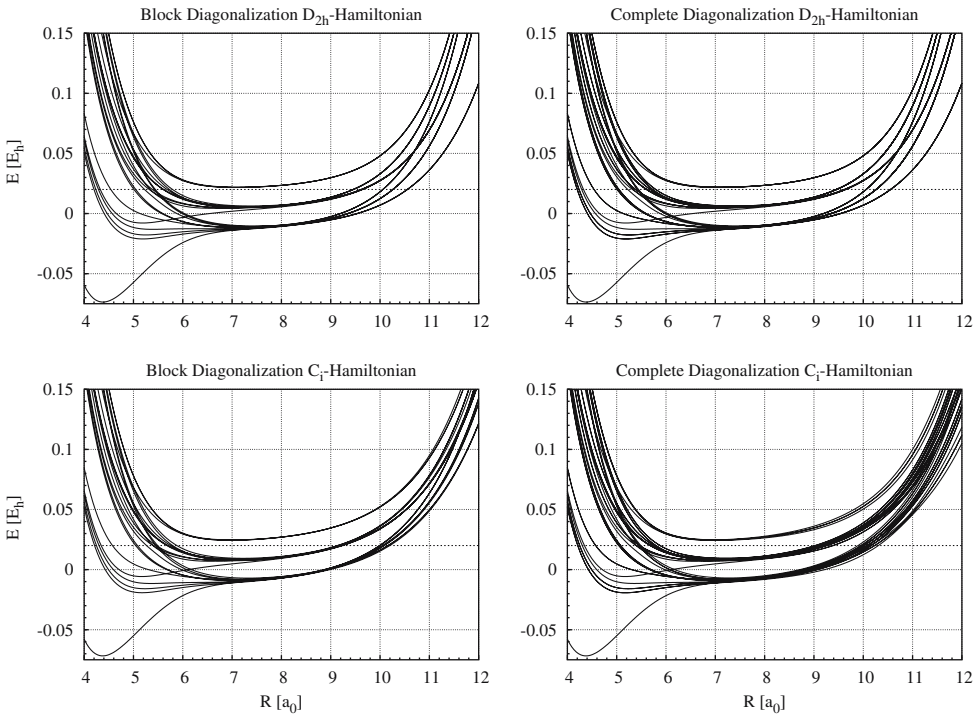

Fig. 5 Manifold of potential energy curves obtained after the first diagonalization step (block-diagonalization) compared to the complete diagonalization (inter-symmetric couplings incorporated) for Br_2 in Ar in D_{2h} and C_i symmetry

each other. In contrast, matrix elements that couple blocks with different symmetries are termed *inter-symmetric* couplings.

The role of this two coupling types can be investigated employing a two-step diagonalization procedure. In the first step the intra-symmetric couplings are accounted for only (pre-diagonalization), in the second step the inter-symmetric couplings are incorporated in order to complete the diagonalization. In Fig. 4, the corresponding potential curves along the Br_2 bond distance obtained from the first diagonalization step are depicted for each symmetry block of the D_{2h}-Hamiltonian. It is seen that the intra-symmetric couplings cause avoided crossings between the potential energy curves within each symmetry block. Moreover, these avoided crossings determine the splitting among that potential energy curves, which would have the same gas phase dissociation limit at large internuclear separations. Note, that the symmetry-based twofold degeneracies of states for $\Omega \neq 0$ are not lifted during this first diagonalization step.

The effect of incorporating the inter-symmetric couplings into the second diagonalization step is shown in Fig. 5, where the manifold of potential energy curves obtained from the first step versus the complete diagonalizion is depicted. Comparing both sets of potential energy curves for the D_{2h}-Hamiltonian one finds almost identical results. Obviously, the inter-symmetric coupling is negligible or even absent here so that we can consider the different symmetry blocks of the Hamiltonian to be approximately independent, even in the rare gas matrix environment.

In addition to the D_{2h} symmetry preserving elongation of the Br_2 bond also its tilting with respect to the ⟨110⟩ direction is of interest reflecting the effect of symmetry breaking. It gives rise to an electronic Hamiltonian of C_i symmetry whose eigenvalues are investigated in the lower panels of Fig. 5 for a tilting of 10° and 5° towards the ⟨100⟩ and ⟨001⟩ directions, respectively. First, we consider the effect of intra-symmetric couplings which is most pronounced for large internuclear separations (>7 a_0) of the Br atoms. As a general trend the intra-symmetric coupling type leads to an enhanced splitting of the potential energy curves. This is to be expected since as compared to the D_{2h} case which is in fact similar to the $D_{\infty h}$ point group of the isolated molecule, the initial two-fold degeneracies are lifted. Including the inter-symmetric couplings into the diagonalization procedure further enhances this effect as shown in the right column of Fig. 5. Nevertheless, it is important to note that one still can consider the interplay of both coupling types independently for the three dissociation limits of the free Br_2 molecule – at least as far as moderate bond length are concerned. Using this separability by dissociation limits together with our knowledge about the two coupling types we are now ready for the targeted reduction of the DIM Hamiltonian matrix.

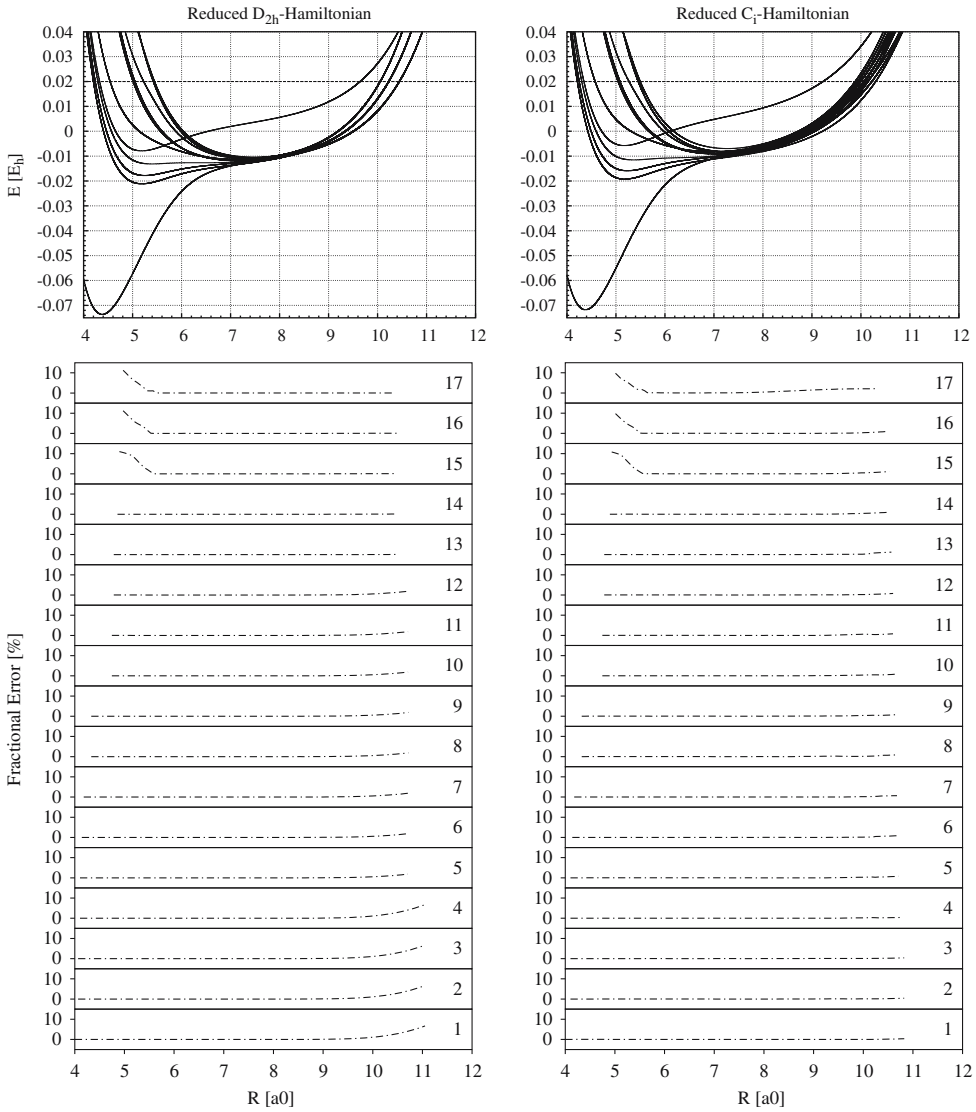

Fig. 6 Comparison of the 17 adiabatic potential energy curves calculated from reduced Hamiltonians for Br_2 in Ar in D_{2h} and C_i symmetry, the *dashed line* denotes the Franck–Condon target energy. The lower two panels show the percentage error with respect to the complete Hamiltonian eigenvalues for energies up to 0.04 Hartree

3.2 A reduced target-state DIM hamiltonian

When we are aiming at a specific reduction of a DIM Hamiltonian towards a model Hamiltonian, the main criterion must be, of course, the phenomenon under investigation, which itself dictates the energy and coordinate range to be addressed. In the following our goal is to taylor a minimal model Hamiltonian for description of the $B \leftarrow X$-state excitation of Br_2 in solid Ar starting from a Franck–Condon vertical transition at the ground state equilibrium bond length. It should be noted though that recent investigations of the B state dynamics (see, e.g., Ref. [33]) start from an excitation into the bound part of the B state PES which is considerably below the vertical Franck–Condon threshold mentioned above and thus well within the target energy range.

Envisaging processes like predissociation and subsequent population of lower lying electronic states we expect that a reduced model shall incorporate all the molecular potential curves which are below to the B-state PES. Accordingly, its basis is defined by the $X(0_g^+)$-, $A'\,(2_u)$-, $A\,(1_u)$-, $^3\Pi_u(0_u^-)$-, $B\,(0_u^+)$-, $C\,(1_u)$-, $^3\Pi_g(2g)$-, $a\,(1_g)$-, $a'\,(0_g^+)$-, $^3\Delta_u(3_u)$- and $1^3\Sigma_u^+\,(0_u^-)$-states. Since such basis set truncation restricts the possible composition of adiabatic states, the validity of the minimal Hamiltonian has to be checked, e.g., by comparing its eigenvalues and eigenvectors to those obtained from its corresponding complete VB representation.

In Fig. 6 the eigenvalues of the reduced D_{2h} and C_i Hamiltonians are shown together with their relative errors with respect to the complete Hamiltonian's eigenvalues. Within the considered energy interval of 0.04 Hartrees, only the upper three eigenvalues in both

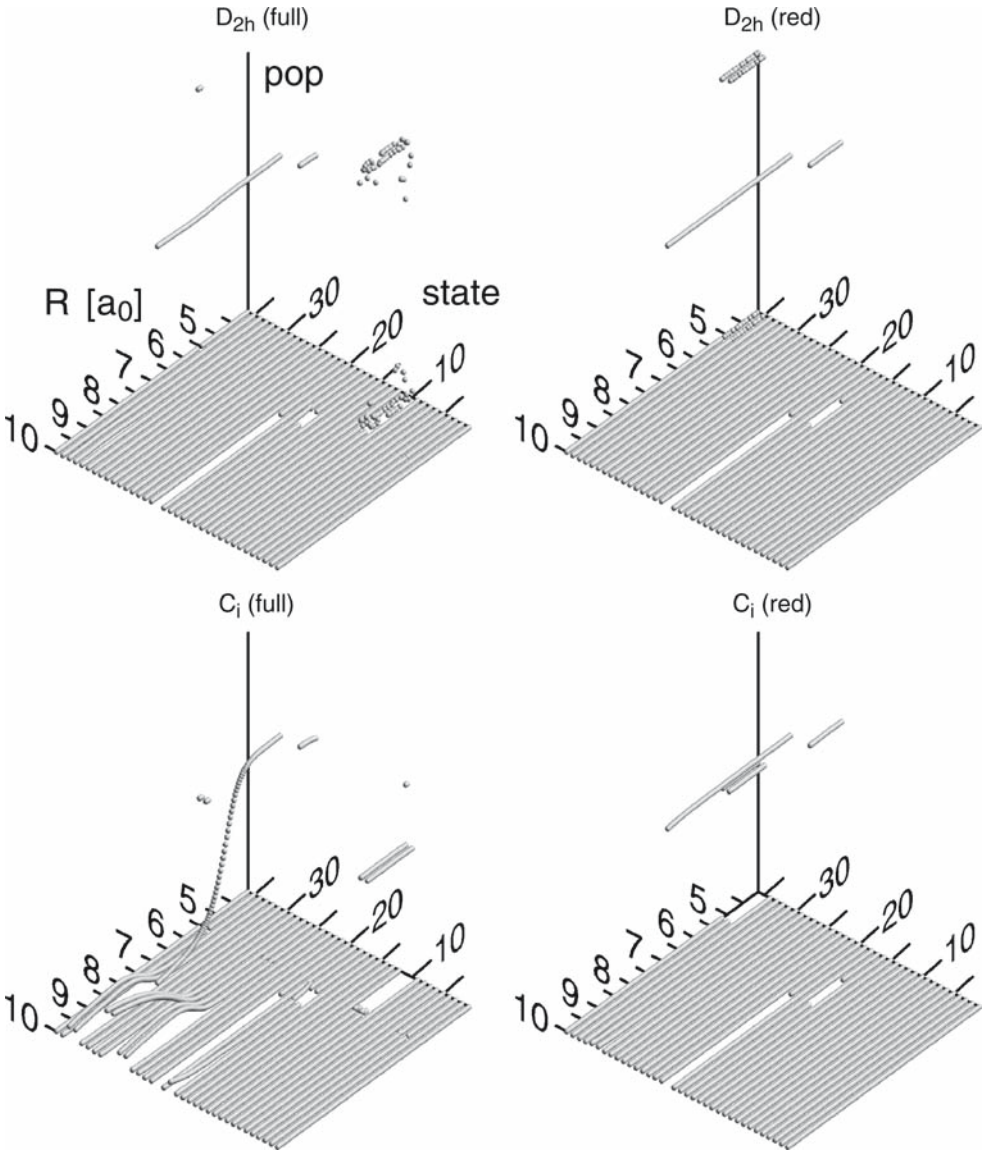

Fig. 7 Composition analysis of the highest adiabatic state of the reduced Hamiltonian obtained by the population of its VB basis functions ordered into symmetry blocks (1–4: 0_g^+, 5: 0_g^-, 6–11: 1_g, 12–15: 2_g, 16–19: 0_u^-, 20: 0_u^+, 21–30: 1_u, 31–34: 2_u, 35–36: 3_u)

cases show significant errors up to 10% at 5 a_0 internuclear distance which vanish for a bond length $\geq 5.5a_0$. At separations beyond 9–10 a_0 the lower four eigenvalues, particularly for the reduced D_{2h} Hamiltonian, deviate from the reference Hamiltonian. However, taking into account that the Franck–Condon vertical transition from electronic ground state with about 0.02 Hartree is far below the given energy interval the performance of both model Hamiltonians is very good.

A more detailed view is provided by a population analysis of the adiabatic eigenvectors in terms of the VB states. Inspired by the overlap criterion of Kuntz et al. [39,46] and based on the subspace representation of our Hamiltonians, we have used the population of single VB basis functions as a measure for the composition of the adiabatics states of the reduced and full Hamiltonians. Exemplary we show in Fig. 7 the results for the adiabatic state that is highest in energy. This state is close to the set of states discarded from the model and we expect mixing effects to be most important here. Inspecting Fig. 7 we notice that the results for the complete and reduced D_{2h}-Hamiltonians agree very well if we take into account that this state falls in the energetically accessible range only after $R > 5.5\,a_0$ (dashed line in Fig. 6). The agreement somewhat deteriorates for the C_i-Hamiltonian. From the populations of the VB states in Fig. 7 we find that the reduced representation resembles the complete one in a bond length range from 5.5

to about 7.5 a_0. Beyond 7.5 a_0 several VB states which are not part of the reduced model start to become populated. However, targeting, for instance, on the initial predissociation the performance of the reduced model is still very good. Note, that the highest adiabatic state is mainly characterized by *B*-state contributions, which itself is the uppermost state by energy within the subspace of chosen basis functions. It further belongs to the second gas phase dissociation limit. In other words, an improved model, say for the C_i case should probably include some more states in this molecular dissociation limit (cf. Table 1).

3.3 B-state predissociation: Br_2 vs. I_2

Finally, it is instructive to focus on the region, where the dissociative potentials cross the *B*-state as shown in Fig. 8. As discussed above this region is particularly well reproduced by the reduced DIM model. The role

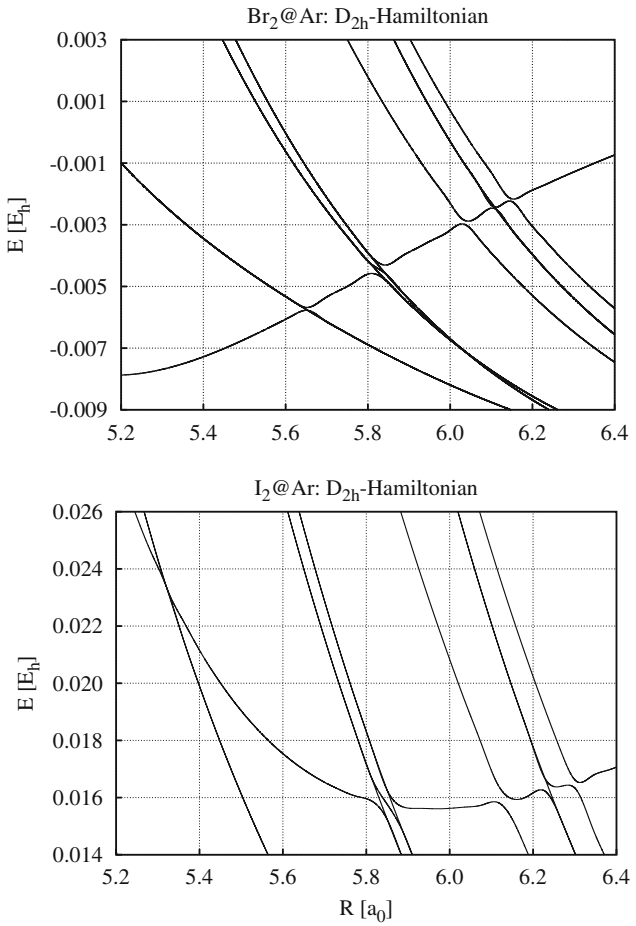

Fig. 8 Close-up view of the crossing region of the $B(0_u^+)$-state with the C (1_u)-, $^3\Pi_g$ $(2g)$-, $a(1_g)$-, a' (0_g^+)-, $^3\Delta_u$ (3_u)- and $1^3\Sigma_u^+$ (0_u^-)-state (*from left to right*) for Br_2 in Ar and I_2 in Ar in D_{2h} symmetry

of these crossings for predissociation of the *B*-state and their dependence on the environmental symmetry has been investigated by Coker et al. [12,47] for molecular iodine in condensed rare gases. Next to Br_2 in Ar we therefore consider I_2 in Ar as a reference case. Adapting the terminology from Ref. [47] we notice that, apart from the different locations of the *B*-state crossings, the pattern of quasi-nonavoided crossings (weakly interacting curves) and avoided crossings (strongly interacting curves) is similar in both systems. On closer examination two common characteristics of these crossings can be found. In case the *B*-state with quantum number $\Omega = 0$ is crossed by a doubly degenerate state with $\Omega \neq 0$, there results *one avoided crossing* and *one non-avoided crossing*. In other words a coupling exists with only one of the degenerate states. The avoided crossing should then give rise to adiabatic dynamics, whereas the nonavoided crossing should give rise to a purely diabatic dissociation dynamics. In case that the *B*-state is crossed by a nondegenerate state with quantum number $\Omega = 0$, there is only an avoided crossing and consequently either bound excited state dynamics or predissociative dynamics are to be expected, depending on whether the halogen molecule follows the upper or the lower one of the resulting adiabatic potential energy curves.

4 Summary

The representation of the halogen, rare gas interaction in a basis of molecular symmetry eigenfunctions allows the grouping of Rg-induced interactions into intra-symmetric and inter-symmetric couplings. Their separate role can be analyzed by a two-step diagonalization scheme as shown in Sect. 3.1. With this classification of coupling types the molecule – rare gas interaction – can be interpreted in terms of molecular Hund's case *c* symmetries, which also form the basis of the selection rules for heavy halogen molecules in gas phase spectroscopy. Based on the leading role of intra-symmetric couplings and the spin–orbit splitting induced energy gap within the symmetry blocks, a separable treatment of the mutual interplay of intra- and inter-symmetric couplings for the three dissociation limits of the isolated molecule becomes possible. This separability facilitates the identification of a relevant set of potential energy curves. Exemplary we have chosen a problem adapted Hamiltonian of reduced complexity for the specific description of the $B \leftarrow X$ excitation and subsequent photodissociation for Br_2 in solid Ar. This model Hamiltonian was found to reasonably reproduce all features of a complete DIM-Hamiltonian within the relevant regime of *B*-state crossings in a comparative study based on the adiabatic

eigenvalues and the composition of adiabatic eigenfunctions. Additionally, the result for Br_2 in Ar were compared to I_2 in Ar as a closely related benchmark system using the same reduction scheme. Of course, the pattern of state crossings is the same in the two cases. However, the overall shifts of the different potential energy curves with respect to each other will lead to a different dynamics, for instance, in predissociation.

The present approach to tailored reduced model Hamiltonians for condensed phase processes shall be particularly relevant for dynamics simulations. Here, it may serve to reduce the numerical effort not only in the quantum domain but also within the framework of quasiclassical surface hopping. Respective work for Br_2 in Ar for which a number of ultrafast spectroscopic experiments have been reported ([2,32,33]) are under way.

Acknowledgments A.B. would like to thank D. F. Coker (Boston) for stimulating discussions as well as for the warm hospitality during a research visit. We are indebted to P. J. Kuntz (Berlin) for drawing our attention to Refs. [39,40,46,48], S. Yabushita as well as Y. Asano (Yokohama) for providing the Br_2 and R. Kosloff as well as J. Vala (Jerusalem) the I_2 gas phase ab initio data. Further, M. V. Korolkov, J. Manz, D. Haase, and M. Gühr (Berlin) are cordially thanked for many insightful conversations. This work has been financially supported by the Deutsche Forschungsgemeinschaft (Sfb450).

Appendix

Table 1 Molecular Hund's Case *c* VB states and their case *a* origins (adapted from Refs. [12,49])

$^{2\Sigma+1}\Lambda_w^\sigma$	Ω_w^σ	$\|JM\rangle_a\|JM\rangle_b$ composition	Dissociation products
$X, 1^1\Sigma_g^+$	0_g^+	$\frac{1}{\sqrt{2}}\left\{\|\frac{3}{2},\frac{1}{2}\rangle_a\|\frac{3}{2},-\frac{1}{2}\rangle_b - \|\frac{3}{2},-\frac{1}{2}\rangle_a\|\frac{3}{2},\frac{1}{2}\rangle_b\right\}$	$^2P_{3/2} +^2 P_{3/2}$
$a', ^3\Sigma_g^-$	0_g^+	$\frac{1}{\sqrt{2}}\left\{\|\frac{3}{2},\frac{3}{2}\rangle_a\|\frac{3}{2},-\frac{3}{2}\rangle_b - \|\frac{3}{2},-\frac{3}{2}\rangle_a\|\frac{3}{2},\frac{3}{2}\rangle_b\right\}$	$^2P_{3/2} +^2 P_{3/2}$
$^3\Pi_g$	0_g^+	$\frac{1}{2}\left\{\|\frac{3}{2},\frac{1}{2}\rangle_a\|\frac{1}{2},-\frac{1}{2}\rangle_b - \|\frac{1}{2},-\frac{1}{2}\rangle_a\|\frac{3}{2},\frac{1}{2}\rangle_b + \|\frac{3}{2},-\frac{1}{2}\rangle_a\|\frac{1}{2},\frac{1}{2}\rangle_b - \|\frac{1}{2},\frac{1}{2}\rangle_a\|\frac{3}{2},-\frac{1}{2}\rangle_b\right\}$	$^2P_{3/2} +^2 P_{1/2}$
$2^1\Sigma_g^+$	0_g^+	$\frac{1}{\sqrt{2}}\left\{\|\frac{1}{2},\frac{1}{2}\rangle_a\|\frac{1}{2},-\frac{1}{2}\rangle_b - \|\frac{1}{2},-\frac{1}{2}\rangle_a\|\frac{1}{2},\frac{1}{2}\rangle_b\right\}$	$^2P_{1/2} +^2 P_{1/2}$
$B', ^3\Pi_u$	0_u^-	$\frac{1}{\sqrt{2}}\left\{\|\frac{3}{2},\frac{3}{2}\rangle_a\|\frac{3}{2},-\frac{3}{2}\rangle_b + \|\frac{3}{2},-\frac{3}{2}\rangle_a\|\frac{3}{2},\frac{3}{2}\rangle_b\right\}$	$^2P_{3/2} +^2 P_{3/2}$
$1^3\Sigma_u^+$	0_u^-	$\frac{1}{\sqrt{2}}\left\{\|\frac{3}{2},\frac{1}{2}\rangle_a\|\frac{3}{2},-\frac{1}{2}\rangle_b + \|\frac{3}{2},-\frac{1}{2}\rangle_a\|\frac{3}{2},\frac{1}{2}\rangle_b\right\}$	$^2P_{3/2} +^2 P_{3/2}$
$^1\Sigma_u^-$	0_u^-	$\frac{1}{2}\left\{\|\frac{3}{2},\frac{1}{2}\rangle_a\|\frac{1}{2},-\frac{1}{2}\rangle_b + \|\frac{1}{2},-\frac{1}{2}\rangle_a\|\frac{3}{2},\frac{1}{2}\rangle_b - \|\frac{3}{2},-\frac{1}{2}\rangle_a\|\frac{1}{2},\frac{1}{2}\rangle_b - \|\frac{1}{2},\frac{1}{2}\rangle_a\|\frac{3}{2},-\frac{1}{2}\rangle_b\right\}$	$^2P_{3/2} +^2 P_{1/2}$
$2^3\Sigma_u^+$	0_u^-	$\frac{1}{\sqrt{2}}\left\{\|\frac{1}{2},\frac{1}{2}\rangle_a\|\frac{1}{2},-\frac{1}{2}\rangle_b + \|\frac{1}{2},-\frac{1}{2}\rangle_a\|\frac{1}{2},\frac{1}{2}\rangle_b\right\}$	$^2P_{1/2} +^2 P_{1/2}$
$^3\Pi_g$	0_g^-	$\frac{1}{2}\left\{\|\frac{3}{2},\frac{1}{2}\rangle_a\|\frac{1}{2},-\frac{1}{2}\rangle_b - \|\frac{1}{2},-\frac{1}{2}\rangle_a\|\frac{3}{2},\frac{1}{2}\rangle_b - \|\frac{3}{2},-\frac{1}{2}\rangle_a\|\frac{1}{2},\frac{1}{2}\rangle_b + \|\frac{1}{2},\frac{1}{2}\rangle_a\|\frac{3}{2},-\frac{1}{2}\rangle_b\right\}$	$^2P_{3/2} +^2 P_{1/2}$
$B, ^3\Pi_u$	0_u^+	$\frac{1}{2}\left\{\|\frac{3}{2},\frac{1}{2}\rangle_a\|\frac{1}{2},-\frac{1}{2}\rangle_b + \|\frac{1}{2},-\frac{1}{2}\rangle_a\|\frac{3}{2},\frac{1}{2}\rangle_b + \|\frac{3}{2},-\frac{1}{2}\rangle_a\|\frac{1}{2},\frac{1}{2}\rangle_b + \|\frac{1}{2},\frac{1}{2}\rangle_a\|\frac{3}{2},-\frac{1}{2}\rangle_b\right\}$	$^2P_{3/2} +^2 P_{1/2}$
$a, ^3\Pi_g$	1_g	$\frac{1}{\sqrt{2}}\left\{\|\frac{3}{2},\frac{3}{2}\rangle_a\|\frac{3}{2},-\frac{1}{2}\rangle_b - \|\frac{3}{2},-\frac{1}{2}\rangle_a\|\frac{3}{2},\frac{3}{2}\rangle_b\right\}$	$^2P_{3/2} +^2 P_{3/2}$
		$\frac{1}{\sqrt{2}}\left\{\|\frac{3}{2},-\frac{3}{2}\rangle_a\|\frac{3}{2},\frac{1}{2}\rangle_b - \|\frac{3}{2},\frac{1}{2}\rangle_a\|\frac{3}{2},-\frac{3}{2}\rangle_b\right\}$	
$^1\Pi_g$	1_g	$\frac{1}{\sqrt{2}}\left\{\|\frac{3}{2},\frac{3}{2}\rangle_a\|\frac{1}{2},-\frac{1}{2}\rangle_b - \|\frac{1}{2},-\frac{1}{2}\rangle_a\|\frac{3}{2},\frac{3}{2}\rangle_b\right\}$	$^2P_{3/2} +^2 P_{1/2}$
		$\frac{1}{\sqrt{2}}\left\{\|\frac{3}{2},-\frac{3}{2}\rangle_a\|\frac{1}{2},\frac{1}{2}\rangle_b - \|\frac{1}{2},\frac{1}{2}\rangle_a\|\frac{3}{2},-\frac{3}{2}\rangle_b\right\}$	
$^3\Sigma_g^-$	1_g	$\frac{1}{\sqrt{2}}\left\{\|\frac{3}{2},\frac{1}{2}\rangle_a\|\frac{1}{2},\frac{1}{2}\rangle_b - \|\frac{1}{2},\frac{1}{2}\rangle_a\|\frac{3}{2},\frac{1}{2}\rangle_b\right\}$	$^2P_{3/2} +^2 P_{1/2}$
		$\frac{1}{\sqrt{2}}\left\{\|\frac{3}{2},-\frac{1}{2}\rangle_a\|\frac{1}{2},-\frac{1}{2}\rangle_b - \|\frac{1}{2},-\frac{1}{2}\rangle_a\|\frac{3}{2},-\frac{1}{2}\rangle_b\right\}$	
$A, ^3\Pi_u$	1_u	$\frac{1}{\sqrt{2}}\left\{\|\frac{3}{2},\frac{3}{2}\rangle_a\|\frac{3}{2},-\frac{1}{2}\rangle_b + \|\frac{3}{2},-\frac{1}{2}\rangle_a\|\frac{3}{2},\frac{3}{2}\rangle_b\right\}$	$^2P_{3/2} +^2 P_{3/2}$
		$\frac{1}{\sqrt{2}}\left\{\|\frac{3}{2},-\frac{3}{2}\rangle_a\|\frac{3}{2},\frac{1}{2}\rangle_b + \|\frac{3}{2},\frac{1}{2}\rangle_a\|\frac{3}{2},-\frac{3}{2}\rangle_b\right\}$	
$C, ^1\Pi_u$	1_u	$\|\frac{3}{2},\frac{1}{2}\rangle_a\|\frac{3}{2},\frac{1}{2}\rangle_b$	$^2P_{3/2} +^2 P_{3/2}$
		$\|\frac{3}{2},-\frac{1}{2}\rangle_a\|\frac{3}{2},-\frac{1}{2}\rangle_b$	
$1^3\Sigma_u^+$	1_u	$\frac{1}{\sqrt{2}}\left\{\|\frac{3}{2},\frac{3}{2}\rangle_a\|\frac{1}{2},-\frac{1}{2}\rangle_b + \|\frac{1}{2},-\frac{1}{2}\rangle_a\|\frac{3}{2},\frac{3}{2}\rangle_b\right\}$	$^2P_{3/2} +^2 P_{1/2}$
		$\frac{1}{\sqrt{2}}\left\{\|\frac{3}{2},-\frac{3}{2}\rangle_a\|\frac{1}{2},\frac{1}{2}\rangle_b + \|\frac{1}{2},\frac{1}{2}\rangle_a\|\frac{3}{2},-\frac{3}{2}\rangle_b\right\}$	

Table 1 continued

$^{2\Sigma+1}\Lambda_w^\sigma$	Ω_w^σ	$\|JM\rangle_a\|JM\rangle_b$ composition	Dissociation products
$2^3\Sigma_u^+$	1_u	$\frac{1}{\sqrt{2}}\left\{\|\frac{3}{2},\frac{1}{2}\rangle_a\|\frac{1}{2},-\frac{1}{2}\rangle_b+\|\frac{1}{2},\frac{1}{2}\rangle_a\|\frac{3}{2},\frac{1}{2}\rangle_b\right\}$	$^2P_{3/2}+^2P_{1/2}$
		$\frac{1}{\sqrt{2}}\left\{\|\frac{3}{2},-\frac{1}{2}\rangle_a\|\frac{1}{2},-\frac{1}{2}\rangle_b+\|\frac{1}{2},-\frac{1}{2}\rangle_a\|\frac{3}{2},-\frac{1}{2}\rangle_b\right\}$	
$^3\Delta_u$	1_u	$\|\frac{1}{2},\frac{1}{2}\rangle_a\|\frac{1}{2},\frac{1}{2}\rangle_b$	$^2P_{1/2}+^2P_{1/2}$
		$\|\frac{1}{2},-\frac{1}{2}\rangle_a\|\frac{1}{2},-\frac{1}{2}\rangle_b$	
$^3\Pi_g$	2_g	$\frac{1}{\sqrt{2}}\left\{\|\frac{3}{2},\frac{3}{2}\rangle_a\|\frac{3}{2},\frac{1}{2}\rangle_b-\|\frac{3}{2},\frac{1}{2}\rangle_a\|\frac{3}{2},\frac{3}{2}\rangle_b\right\}$	$^2P_{3/2}+^2P_{3/2}$
		$\frac{1}{\sqrt{2}}\left\{\|\frac{3}{2},-\frac{3}{2}\rangle_a\|\frac{3}{2},-\frac{1}{2}\rangle_b-\|\frac{3}{2},-\frac{1}{2}\rangle_a\|\frac{3}{2},-\frac{3}{2}\rangle_b\right\}$	
$^1\Delta_g$	2_g	$\frac{1}{\sqrt{2}}\left\{\|\frac{3}{2},\frac{3}{2}\rangle_a\|\frac{1}{2},\frac{1}{2}\rangle_b-\|\frac{1}{2},\frac{1}{2}\rangle_a\|\frac{3}{2},\frac{3}{2}\rangle_b\right\}$	$^2P_{3/2}+^2P_{1/2}$
		$\frac{1}{\sqrt{2}}\left\{\|\frac{3}{2},-\frac{3}{2}\rangle_a\|\frac{1}{2},-\frac{1}{2}\rangle_b-\|\frac{1}{2},-\frac{1}{2}\rangle_a\|\frac{3}{2},-\frac{3}{2}\rangle_b\right\}$	
$A',^3\Pi_u$	2_u	$\frac{1}{\sqrt{2}}\left\{\|\frac{3}{2},\frac{3}{2}\rangle_a\|\frac{3}{2},\frac{1}{2}\rangle_b+\|\frac{3}{2},\frac{1}{2}\rangle_a\|\frac{3}{2},\frac{3}{2}\rangle_b\right\}$	$^2P_{3/2}+^2P_{3/2}$
		$\frac{1}{\sqrt{2}}\left\{\|\frac{3}{2},-\frac{3}{2}\rangle_a\|\frac{3}{2},-\frac{1}{2}\rangle_b+\|\frac{3}{2},-\frac{1}{2}\rangle_a\|\frac{3}{2},-\frac{3}{2}\rangle_b\right\}$	
$b',^3\Delta_u$	2_u	$\frac{1}{\sqrt{2}}\left\{\|\frac{3}{2},\frac{3}{2}\rangle_a\|\frac{1}{2},\frac{1}{2}\rangle_b+\|\frac{1}{2},\frac{1}{2}\rangle_a\|\frac{3}{2},\frac{3}{2}\rangle_b\right\}$	$^2P_{3/2}+^2P_{1/2}$
		$\frac{1}{\sqrt{2}}\left\{\|\frac{3}{2},-\frac{3}{2}\rangle_a\|\frac{1}{2},-\frac{1}{2}\rangle_b+\|\frac{1}{2},-\frac{1}{2}\rangle_a\|\frac{3}{2},-\frac{3}{2}\rangle_b\right\}$	
$^3\Delta_u$	3_u	$\|\frac{3}{2},\frac{3}{2}\rangle_a\|\frac{3}{2},\frac{3}{2}\rangle_b$	$^2P_{3/2}+^2P_{3/2}$
		$\|\frac{3}{2},-\frac{3}{2}\rangle_a\|\frac{3}{2},-\frac{3}{2}\rangle_b$	

References

1. Apkarian VA, Schwentner N(1999) Chem Rev 99:1481
2. Gühr M, Ibrahim H, Schwentner N (2004) Phys Chem Chem Phys 6:5353
3. Fushitani M, Bargheer M, Gühr M, Schwentner N (2005) Phys Chem Chem Phys 7:3143
4. Fushitani M, Schwentner N, Schröder M, Kühn O (2006) J Chem Phys 124:024505
5. Jungwirth P, Gerber RB (1999) Chem Rev 99:1583
6. May V, Kühn O (2004) Charge and energy transfer dynamics in molecular systems, 2nd revised and enlarged edn. Wiley–VCH, Weinheim
7. Ellison FO (1963) J Am Chem Soc 85:3540
8. Tully JC (1973) J Chem Phys 58:1396
9. Tully JC (1973) J Chem Phys 59:5122
10. Gersonde IH, Gabriel H (1993) J Chem Phys 98:2094
11. Lawrence WG, Apkarian VA (1994) J Chem Phys 101:1820
12. Batista VS, Coker DF (1996) J Chem Phys 105:4033
13. Batista VS, Coker DF (1997) J Chem Phys 106:6923
14. Batista VS, Coker DF (1997) J Chem Phys 106:7102
15. Krylov A, Gerber RB (1997) J Chem Phys 106:6574
16. Niv MY, Bargheer M, Gerber RB (2000) J Chem Phys 113:6660
17. Grigorenko BL, Nemukhin AV, Apkarian VA (1997) Chem Phys 219:161
18. Grigorenko BL, Nemukhin AV, Buchachenko AA, Stepanov NF, Umanskii SY (1997) J Chem Phys 106:4575
19. Grigorenko BL, Nemukhin AV, Ozhegova NV (1998) Chem Phys Lett 296:84
20. Buchachenko AA, Stepanov NF (1996) J Chem Phys 104:9913
21. Buchachenko AA, Stepanov NF (1996) Chem Phys Lett 261:591
22. Buchachenko AA (1998) Chem Phys Lett 292:273
23. de Lara-Castells MP, Buchachenko AA, Delgado-Barrio G, Villarreal P (2003) J Chem Phys 120:2182
24. Kiljunen T, Bargheer M, Gühr M, Schwentner N (2004) Phys Chem Chem Phys 6:2185
25. Kiljunen T, Bargheer M, Gühr M, Schwentner N, Schmidt B (2004) Phys Chem Chem Phys 6:2932
26. Bargheer M, Gerber RB, Korolkov MV, Kühn O, Manz J, Schröder M, Schwenter N (2002) Phys Chem Chem Phys 4:5554
27. Gerber RB, Korolkov MV, Manz J, Niv MY, Schmidt B (2000) Chem Phys Lett 327:76
28. Chaban G, Gerber RB, Korolkov MV, Manz J, Niv MY, Schmidt B (2001) J Phys Chem A 105:2770
29. Alekseyev AB, Korolkov MV, Kühn O, Manz J, Schröder M (2006) J Photochem Photobiol A 180:262
30. Margulis CJ, Coker DF (2001) J Chem Phys 114:6744
31. Belyaev AK, Tiukanov AS, Domcke W (2001) Phys Rev A 65:012508
32. Gühr M, Schwentner N (2005) J Chem Phys 123:244506
33. Gühr M, Schwentner N (2005) Phys Chem Chem Phys 7:760
34. Asano Y, Yabushita S (2003) Chem Phys Lett 372:348
35. Herzberg G (1950) Molecular spectra and molecular structure I. Spectra of diatomic molecules, Van Nostrand Reinhold, New York
36. Chang TY (1967) Rev Mod Phys 39:911
37. Umanskij SJ, Nikitin EE (1969) Theor Chim Acta 13:91
38. Lefebvre-Brion H, Field RW (2004) The spectra and dynamics of diatomic molecules, Elsevier, Amsterdam
39. Schreiber JL, Kuntz PJ (1982) J Chem Phys 76:1872
40. Kuntz PJ, Schreiber JL (1982) J Chem Phys 76:4120
41. Casavecchia P, He G, Sparks RK, Lee YT (1981) J Chem Phys 75:710

42. Zhao Y, Yourshaw I, Reiser G, Arnold CC, Neumark DM (1994) J Chem Phys 101:6538
43. Yourshaw I, Zhao Y, Neumark DM (1996) J Chem Phys 105:351
44. Yabushita S Private communication
45. Becker CH, Casavecchia P, Lee YT, Olsen RE, Lester WE (1979) J Chem Phys 70:5477
46. Poliák R, Paidarová I, Kuntz PJ (1985) J Chem Phys 82:2352
47. Yu N, Margulis CJ, Coker DF (2001) J Phys Chem B 105:6728
48. Gadea FX, Kuntz PJ (1988) Mol Phys 63:27
49. Saute M, Aubert-Frécon M (1982) J Chem Phys 77:5639